AIP Conference Proceedings

Finite element analysis of stress transfer mechanism from matrix to the fiber in SWCN reinforced nanocomposites

Cite as: AIP Conference Proceedings **1809**, 020021 (2017); https://doi.org/10.1063/1.4975436
Published Online: 24 February 2017

E. Günay

View Online Export Citation

ARTICLES YOU MAY BE INTERESTED IN

Mechanical properties of single layer graphene nanoribbons through bending experimental simulations
AIP Advances **4**, 031333 (2014); https://doi.org/10.1063/1.4868625

Experimental analysis of electrical properties of composite materials
AIP Conference Proceedings **1809**, 020016 (2017); https://doi.org/10.1063/1.4975431

Simplified equation for Young's modulus of CNT reinforced concrete
AIP Advances **7**, 125122 (2017); https://doi.org/10.1063/1.5011319



AIP Publishing

© 2017 Author(s).

Corrigendum: *Finite Element Analysis of Stress Transfer Mechanism from Matrix to the Fiber in SWCN Reinforced Nanocomposites*, E. Günay, AIP Conf. Proc. **1809**, 020021 (2017)

Figures, 16, 17, and 18 of the original article PDF file, as supplied to AIP Publishing, were affected by a PDF-processing error. Consequently, a solid diamond symbol appeared instead of a Greek tau on the *y* axis labels for these three figures. This article was updated on 17 March 2017 to correct the PDF-processing error, with the scientific content remaining unchanged.

Finite Element Analysis of Stress Transfer Mechanism from Matrix to the Fiber in SWCN Reinforced Nanocomposites

E. Günay

Gazi University, Engineering Faculty, Mechanical Engineering Department, 06570, Maltepe, Ankara, Turkey
Corresponding author: ezgigunay@gazi.edu.tr

Abstract. This study defined as micromechanical finite element (FE) approach examining the stress transfer mechanism in single-walled carbon nanotube (SWCN) reinforced composites. In the modeling, 3D unit-cell method was evaluated. Carbon nanotube reinforced composites were modeled as three layers which comprises CNT, interface and matrix material. Firstly; matrix, fiber and interfacial materials all together considered as three layered cylindrical nanocomposite. Secondly, the cylindrical matrix material was assumed to be isotropic and also considered as a continuous medium. Then, fiber material was represented with zigzag type SWCNs. Finally, SWCN was combined with the elastic medium by using springs with different constants. In the FE modeling of SWCN reinforced composite model springs were modeled by using ANSYS spring damper element COMBIN14. The developed interfacial van der Waals interaction effects between the continuous matrix layer and the carbon nanotube fiber layer were simulated by applying these various spring stiffness values. In this study, the layered composite cylindrical FE model was presented as the equivalent mechanical properties of SWCN structures in terms of Young's modulus. The obtained results and literature values were presented and discussed.

Keywords: Nanotechnology; Carbon nanotube; Fiber-reinforced composites; Interfaces; Finite element analysis.
PACS: 81.07.-b, 61.48.De, 81.05.Ni, 68.35.-p, 02.70.Dh.

INTRODUCTION

Macro and micro studies were evaluated numerically and experimentally, the results were compared as possible. In the literature survey, nano-composites were designed as various forms of multi-layered nano-composites. These multilayered composites were composed of three layers in cylindrical form. These layers were named as follows: matrix material, interface material and fiber material. Each layer consists of a different material type and shows its own physical properties. In the literature, various numerical models were developed appropriate to the structure material in order to find the real structural properties of these layers. Typical bonding methods were used to combine the matrix and fiber in the most suitable form. Considering the researches performed in recent years; single or double-layered carbon nanotubes were seen as a model for fiber reinforcing material. The objective of the

Proceedings of the 6th International Advances in Applied Physics and Materials Science Congress & Exhibition
AIP Conf. Proc. 1809, 020021-1–020021-18; doi: 10.1063/1.4975436
Published by AIP Publishing. 978-0-7354-1477-8/$30.00

most recent studies was to create a new modeling to measure the stress transfer mechanism from fiber to matrix in which the fibers were properly connected.

Basic models were performed using the finite element method. Ruoff et al. [1] investigated the tensile and bending stiffness constants of ideal multi-walled (MWCNT) and single-walled carbon nanotubes (SWCNT) in terms of the known elastic properties of graphite. A semi-continuum finite element approach to evaluate the Young's modulus of single-walled carbon nanotube reinforced composites was investigated by Giannopoulos et al. [2]. In order to accomplish this, a cylindrical representative volume element (RVE) was employed with reinforcement by single walled CNT, the interfacial region represented by spring joint elements and the continuum matrix region by epoxy material. Investigation of stress transfer in carbon nanotube reinforced composites using a multi-scale finite element approach was performed by Spanos et al. [3, 4]. The computation of the elastic mechanical properties of graphene sheets, nanoribbons and graphite flakes using spring based finite element model was performed by Georgantzinos et al. [5]. Shokrieh et al. [6, 7] reported that bonding between carbon nanotube and its surrounding polymer was treated as van der Waals interaction. The results about simulation of carbon nanotube reinforced polymer suggested a non-linear stress-strain behaviour. An equivalent fiber was obtained to calculate the elastic constants of the composite. Wan et al. [8] investigated the effect of CNT length and CNT-matrix interface in single walled carbon nanotube (SWCNT) reinforced composites using continuum model. Zhou et al. [9] reported that the van der Waals pressure between two layers of double walled carbon nanotubes (DWCNT) was introduced in the model, and the Poisson's effects of DWCNT and the matrix were also taken into account by the generalized Hooke's law. Needleman et al. [10] reported that the presence of an interface increased the composite stiffness. However, this interface caused separation and ultimately reduced the stress bearing capacity of the composite. Tsai et al. [11] investigated the characterization of the fracture parameters of a graphene sheet using atomistic simulation and continuum mechanics. Ruoff et al. [12] discussed the mechanical properties of carbon nanotubes by theoretical predictions and experimental measurements. Delmotte et al. [13] reviewed the mechanical properties of carbon nanotubes. Pantano et al. [14] studied on the mechanics of deformation of single and multi-wall carbon nanotubes. Individual tubes were modeled using shell elements, where a specific pairing of elastic properties and mechanical thickness of tube wall were identified to enable successful modeling with shell theory.

The aim of this study was to investigate the effects of spring joint elements as an interface material on the calculation of Young's modulus and the determination of the interface stresses for SWCN reinforced nanotube. The matrix material in tubular form was selected from a homogeneous and continuum medium.The matrix material is being selected from a homogeneous and continuum medium and it has been defined in tubular form. In this research the selected matrix material was epoxy resin. Beside this, fiber material was defined as the discontinuous single walled zigzag type carbon nanotube (SWCN). Two different zigzag type nanotubes (5,0,20) and (20,0,20) were introduced as a fiber geometry and material. Matrix and fiber geometries were connected to each other with the help of springs in place of van der Waals bonds. The

developed interfacial van der Waals interaction effects between the matrix layer and the carbon nanotube fiber layer were simulated by finite element method.

MICROMECHANICAL MODELLING

All of the computations were performed in a representative volume element (RVE) which consists of matrix, interface joint spring elements and single wall carbon nanotube (Fig. 1). The geometric parameters of the RVE were determined from the Eqn. 1 and Eqn. **2** given as below. In these equations V_n, V_{CNT}, V_m were the volume fractions of the CNT in the composite with respect to the proposed RVE, volume fraction of the nanotube and volume fraction of matrix material respectively. The parameters r_n, r_m presented the radius of the nanotube and matrix, t_n the nanotube with 0.34 nm wall thickness [2, 15] ; l_n represented the nanotube length. $E_c\left(\because E_c^*\right)$ showed the Young's modulus of the nanocomposite which was approximately predicted by Eqn. 2. In this study, construction of the fiber-reinforced composite structure was formed with the combination of the carbon nanotube and joint-springs in order to represent the fiber structure. The interface between matrix and carbon nanotubes was represented with the help of different number of springs with high stiffness properties. By applying this equation (**R**ule of **M**ixtures: ROM) effective Young's modulus of the fiber-reinforced composite was estimated in the fiber direction.

$$V_n = \frac{V_{CNT}}{V_{matrix}+V_{CNT}} = \frac{2\pi r_n t_n l_n}{\left\{\pi\left[r_m^2-(r_n+t_n/2)^2\right]l_n+2\pi r_n t_n l_n\right\}} = \frac{8 r_n t_n}{4r_m^2-(t_n-2r_n)^2} \tag{1}$$

$$E_c = E_n V_n + (1-V_n)E_m \tag{2}$$

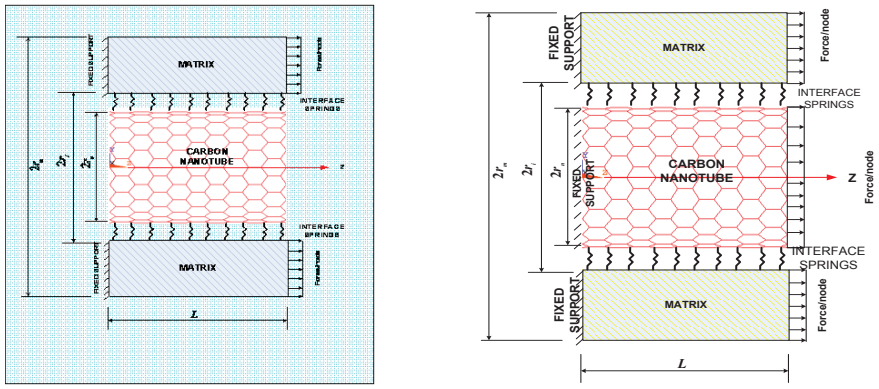

a) b)

Figure 1. Representative volume element (RVE) of zigzag type carbon nanotube with joint-springs reinforced composite: a) BC_1: loading applied from matrix; b) BC_2: loading applied from both matrix and carbon nanotube.

The radius of matrix r_m was solved using the Eqn. 1 with corresponding volume fractions of 1%-4%. The calculated Young's modulus and radii values of the zigzag nanotubes (5,0,20) (Fig. 2), (20,0,20) (Fig. 3) were $E_n = 0.961TPa$, $r_n = 1.9586A^\circ$ and $E_n = 1.035TPa$, $r_n = 9.535A^\circ$ respectively (Table 1, Table 2).

Table 1. FE models with zigzag (5,0,20) type carbon nanotube and number of elements with their types.

Volume Fraction $(V_n)\%$	**Radius of the matrix** $(r_m)\,A^\circ$	**Mesh elements (Matrix) SHELL181**	**Mesh elements (Reinforcing Springs) COMBIN14**	**Mesh elements (Carbon nanotube) BEAM4**
1	11.543	1105	103	145
2	8.165	639, 3159	120, 580	145, 121
3	6.668	599	99	145
4	5.780	479	99	145

Table 2. FE models with zigzag (20,0,20) type carbon nanotube and number of elements with their types.

Volume Fraction $(V_n)\%$	**Radius of the matrix** $(r_m)\,A^\circ$	**Mesh elements (Matrix) SHELL181**	**Mesh elements (Reinforcing Springs) COMBIN14**	**Mesh elements (Carbon nanotube) BEAM4**
1	80.755	3626	138	580
2	57.474	7902	447	580
3	47.145	2059	166	580
4	41.016	2819	221	580

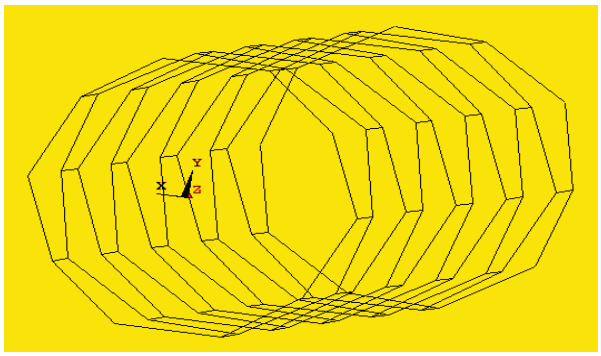

Figure 2. Meshing of zigzag (5,0,20) type carbon nanotube.

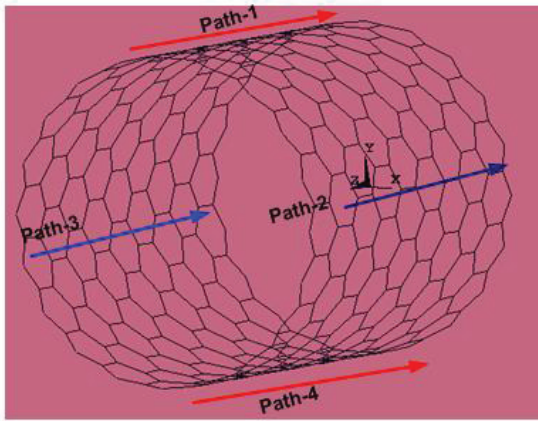

Figure 3. Meshing of zigzag (20,0,20) type carbon nanotube.

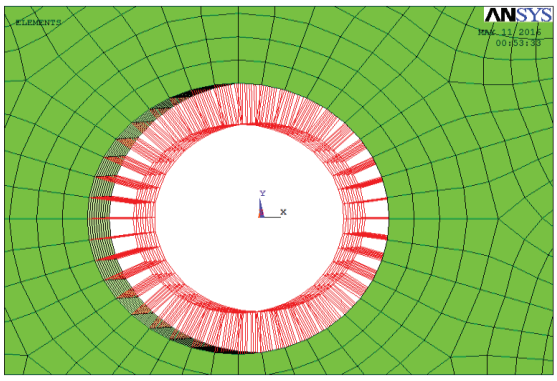

Figure 4. Zigzag (20,0,20) type nanotube-Combin14 spring elements -Shell181 mesh elements combination (Young's modulus of the nanotube $E_n = 1.035TPa$, radius of the nanotube $r_n = 9.535A^{\circ}$, $(V_n)\% = 2$).

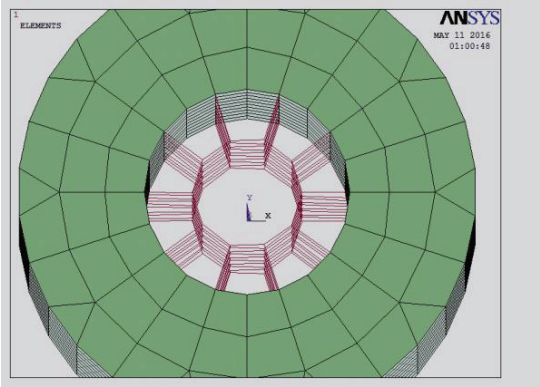

Figure 5. Zigzag (5,0,20) type nanotube-Combin14 spring elements -Shell181 mesh elements combination (Young's modulus of the nanotube $E_n = 0.961 TPa$, radius of the nanotube $r_n = 1.9586 A^{\circ}$, $(V_n)\% = 2$).

Carbon nanotubes were generated from two-nodes **BEAM 3-D elastic 4** element with the properties given in detail in Table 3 [16, 17] (Fig. 2, Fig. 3). Element has six degrees of freedom per node (UX, UY, UZ, ROTX, ROTY, ROTZ). Carbon nanotube elastic constants were calculated as $k_{carbon} = 0.961\ TPa$ and $k_{carbon} = 1.035 TPa$. The thickness of the interface section was equal to one half of the wall thickness of the nanotube $(t_n/2)$ [2, 15], and usually taken as equal to 3.4 Å. The matrix section of the composite was considered to be a continuous structure such as epoxy material, and comparison of the results were done for three different values of elstic constants of matrix material (Table 4). $E_{matrix} = k_{matrix} = 3GPa$, $E_{matrix} = k_{matrix} = 30\,GPa$ and $E_{matrix} = k_{matrix} = 300\,GPa$ (Table 4). The matrix was modelled by using four-node linear mesh element **SHELL181** with six degrees of freedom per node (UX, UY, UZ, ROTX, ROTY, ROTZ) (Fig. 4). **COMBIN14** mesh element has three degrees of freedom per node (UX, UY, UZ) (Fig. 5). Stiffness value of the springs was chosen as $k_{spring} = k_s = 1.33\ TPa$ and this value was defined for **COMBIN14** mesh element. Finite element analyses were performed for five different stiffness ratios as,

$$k_i/k_s = 2.255\times10^{-3},\ 2.255\times10^{-2},\ 2.255\times10^{-1},\ 3.1217\times10^{-3},\ 2.8985\times10^{-3}$$

(Table 5, Table 6).

Table 3. Carbon nanotube BEAM 3-D Elastic-4 beam section properties.

A	1.697e-8 A° ^{2}
I_{zz}	0.227 A° ^{4}
I_{yy}	0.227 A° ^{4}
t_z	0.147 A° ^{4}
t_y	0.147 A° ^{4}
I_{xx}	0.453 A° ^{4}
E_x	5.49e-8 N/A°^{2}
E_y	5.49e-8 N/A°^{2}
E_z	5.49e-8 N/A°^{2}
G_{xy}	8.71 e-9 N/A°^{2}
G_{yx}	8.71 e-9 N/A°^{2}
G_{xz}	8.71 e-9 N/A°^{2}

COMPUTATIONAL PROCEDURES

This study was performed mainly in two steps. In the first step, the Young's modulus of the nanocomposite structure was calculated in which the composite structure was loaded axially. At one end of the cylinder (RVE) only the nodes of the matrix profile were fully restrained, i.e., the degrees of freedom of all nodes of this surface were restricted. At the other end of the cylinder (RVE), a constant force per node was applied at the nodes of the circular cross sectional face of the matrix (Fig. 1(a)). The back and front faces of the carbon nanotube were neither supported nor loaded, they were released free of loading (Boundary Condition type 1: BC_1). By this way it was allowed the stiffness effect of the carbon nanotube to be transferred to the matrix through the interconnection springs. The Young's modulus value of the nanocomposite was calculated from the ANSYS code nodal solution with the replacement of the values in the following Hooke's formula:

$$E_c = \left[\frac{\left(\sigma_z^{node}\right)_{max}}{\left(\varepsilon_z^{node}\right)_{max}} \right]_{Loaded\ face} \tag{3}$$

In the second stage of this study, stress distribution formed between the matrix and carbon nanotube was calculated under the similar axial loading applications. At one end of the cylinder (RVE) both the nodes of the matrix profile and carbon nanotube were fully restrained, i.e. the degrees of freedom of all nodes of this surface were restricted (Boundary Condition type 2: BC_2). At the other end of the RVE, nanocomposite was loaded with a constant force per node (Fig. 1(b)).

FE ANALYSIS RESULTS

The first step in application was performed with the boundary condition BC_1 and $V_n(1\%-4\%)$ type nanocomposite cylinders. The results obtained from the modeling and analysis can be viewed from in the Table 4 and Table 5. The curves of these data have shown in the Figure 6 and Figure 7. The elastic constant of the matrix material was considered as $E_{matrix}=3GPa$ then, the values obtained from FEM model and the ROM model (E_{ROM}/E_m) were compared with each other. According to this comparison $4.5-18.5$ relative difference was found between them. . By proceeding ROM model and the matrix material with Young's modulus on the same curve, the proportion of these two values was found and the curve was plotted. Approximate difference between the ROM model and the matrix material was $0.98-1.2$ .The increasing difference between the FEM model and ROM model was found to be proportional to the increase in the volume fraction of fiber in matrix. The increasing difference between the FEM model and ROM model was found to be proportional to the increase in the value of the volume fraction of fiber in matrix. These results were found to be consistent with the literature [2]. Zigzag (5,0,20) and zigzag (20,0,20) carbon nanotubes gave similar results in terms of the equivalent elastic constants of nanocomposite structures. The differences obtained by studying the two reinforcing structures that affected the general structure of the composite was shown in Fig. 7. The equivalent composite elastic constants obtained from FE analysis by inserting the matrix material elastic constants $3GPa$, $30GPa$ and $300GPa$ were shown in Fig. 8 respectively. According to these results it was found that, when the matrix material has the largest elastic constant ($300GPa$) both the carbon nanotube model and the ROM model have shown aproximately same values. The differences caused by the selected carbon nanotube reinforced composite structure have been observed between $1-1.2$ factors $(E_{matrix}=3GPa)$ (Fig.9).

According to our results, the biggest effects developed on the equivalent elastic constant of the reinforced nanocomposite have obtained from the following parameters; (i) the equivalent elastic constant value of carbon nanotube, (ii) the number of series of joint spring elements and their corresponding stiffness values, (ii) the defined matrix material with its geometrical and material properties (Figs. 6-9).

The stress (σ_z), strain (ε_z), and displacement (δ_z) based curves obtained from Ansys code for zigzag (20,0,20) type nanotube (Young's modulus of the nanotube: $E_n=1.035TPa$, radius of the nanotube: $r_n=9.535A^\circ$, $\left(r_m=5.780A^\circ\right),(V_n=4\%)$) have been shown in Figures 10-14. The developing z directional stress distribution plots (σ_z) on the unrestricted (BC_1,Fig.1(a)) reinforced nanocomposite as; $3GPa$, $30GPa$ and $300GPa$ matrix models have been shown in Figures 10, 11 and 12 respectively. The strain distribution (ε_z) for $300GPa$ has been shown in Figure 13, the z directional displacement distribution for $300GPa$,(δ_z) has been shown in Fig. 14 and the δ_z -displacement distribution of restrained (BC_2, Fig. 1(b)) nanocomposite for $E_m=300GPa$ (zigzag (20,0,20) type nanotube (Young's modulus of the nanotube: $E_n=1.035TPa$, radius of the nanotube: $r_n=9.535A^\circ$, $\left(r_m=8.165A^\circ\right),(V_n=2\%)$) has

been shown in Fig. 15. As seen in Figure 14 and Figure 15, the relative minimum value of the z-displacement (δ_z) occured in the interface region where the joint-springs were aligned there. The other results obtained from the examination of interface shear stress distribution (τ_{rz}) by applying the second type of boundary condition (BC_2) on the FE model by have been shown in Figs. 16, 17 and 18. Figure 16 has shown clearly the interfacial shear stress distribution formed between the matrix and carbon nanotube [18]. The plotted nodal shear stress values were obtained from nodal solution of matrix section (Shell181 elements) while the corresponding axial stresses obtained from the carbon nanotube by ANSYS Beam-4 elements at same locations of the meshing system. As it is shown in the Figs. 16, 17 and 18, the carrying capacity of the matrix was found to be 33.3% of the total load carrying capacity of the modelled composite structure. The load carrying capacity of the springs and carbon nanotube together was 66.7% of the overall load carrying capacity of the modeled composite structure.

Table 4. FEA results for zigzag (5,0,20) type nanotube (Young's modulus of the nanotube $E_n = 0.961TPa$, radius of the nanotube $r_n = 1.9586A^\circ$).

Volume Fraction $(V_n)\%$	**Present model** $E_c(GPa)$	**Rule of mixtures** $E_c^*(GPa)$	**Matrix material** $E_m(GPa)$	**Elastic constants ratio** E_c^*/E_c
1	3.205	12.58	3.0	3.925
2	3.1013	22.16	3.0	7.145
3	3.569	31.74	3.0	8.893
4	2.946	41.32	3.0	14.026

Table 5. FEA results for zigzag (20,0,20) type nanotube (Young's modulus of the nanotube $E_n = 1.035TPa$, radius of the nanotube $r_n = 9.535A^\circ$).

Volume Fraction $(V_n)\%$	**Present model** $E_c(GPa)$	**Rule of mixtures** $E_c^*(GPa)$	**Matrix material** $E_m(GPa)$	**Elastic constants ratio** E_c^*/E_c
1	2.398	13.32	3.0	5.555
2	3.409	23.64	3.0	6.935
3	3.379	33.96	3.0	10.050
4	3.324	44.28	3.0	13.321

Table 6. FEA results for zigzag (20,0,20) type nanotube (Young's modulus of the nanotube $E_n = 1.035TPa$, radius of the nanotube $r_n = 9.535A^\circ$ and volume fractions; $V_n = 4\%$, $V_n = 2\%$).

Matrix material $E_m(GPa)$	**Present model** $V_n = 2\%$ $E_c(GPa)$	**Present model** $V_n = 4\%$ $E_c(GPa)$	**Rule of mixtures** $E_c^*(GPa)$	**Elastic constants ratio** $V_n = 2\%$ E_c^*/E_c	**Elastic constants ratio** $V_n = 4\%$ E_c^*/E_c
3	3.48	3.19	44.28	6.79	13.88
30	34.69	34.22	70.20	1.16	2.05
300	345.54	345.0	329.4	0.91	0.96

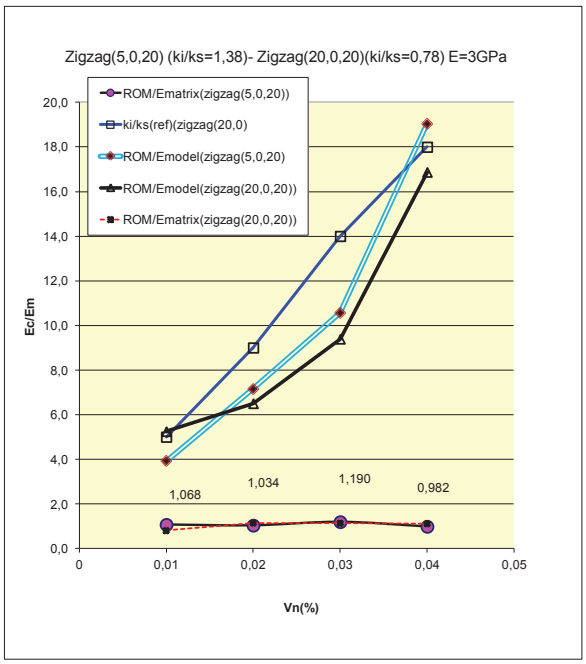

Figure 6. Comparison of **FEA** results ROM/E_{matrix} and ROM/E_{model} versus volume fraction $(V_n\%)$ for zigzag (5,0,20) and (20,0,20) type reinforced nanocomposites.

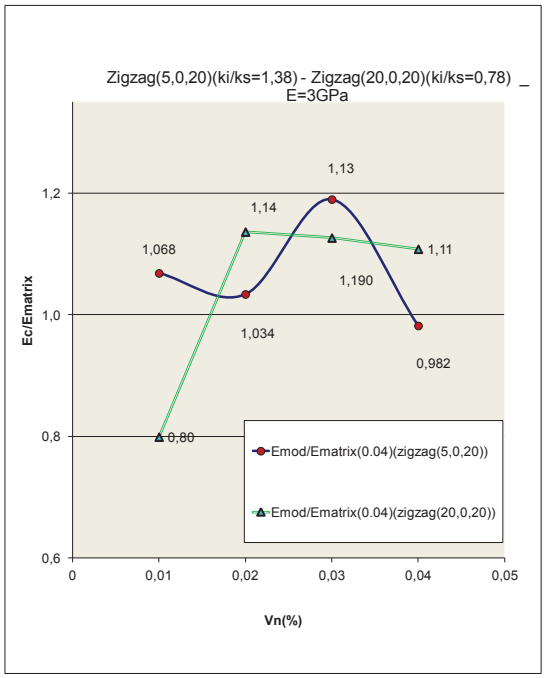

Figure 7. Comparison of the FEA results for E_{model}/E_{matrix} versus volume fraction $(V_n\%)$ for zigzag (5,0,20) and (20,0,20) type reinforced nanocomposites.

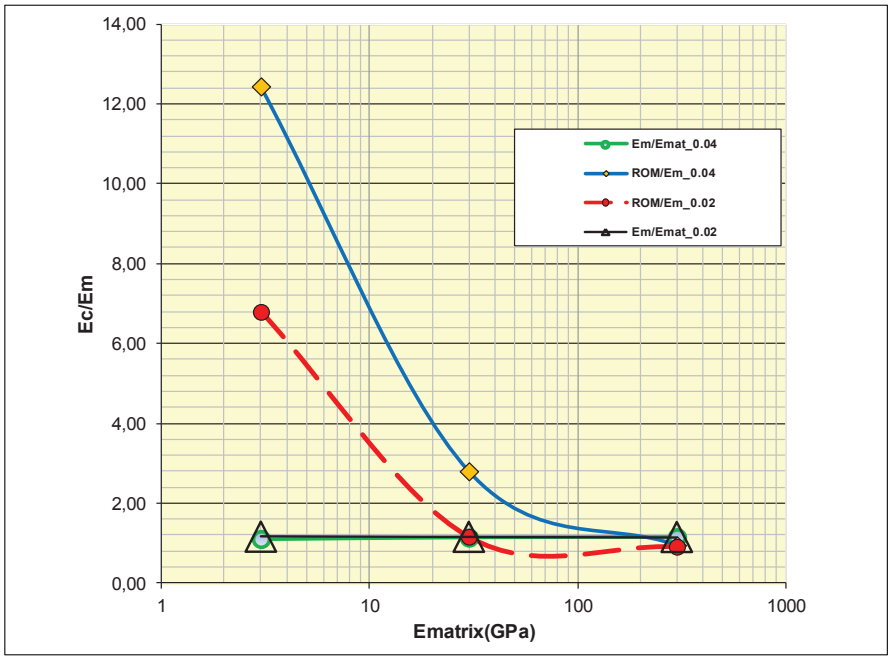

Figure 8. Comparison of FEA results ROM/E_{matrix} and ROM/E_{model} versus E_{matrix} for zigzag (5,0,20) and zigzag(20,0,20) type reinforced nanocomposites.

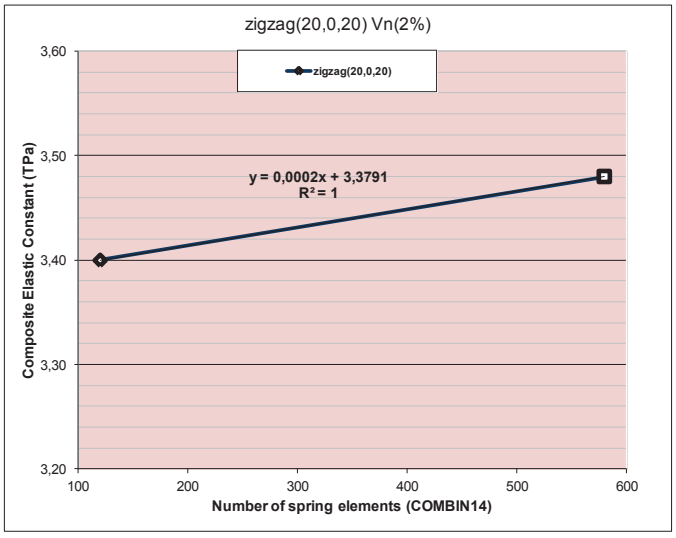

Figure 9. Variation of Young's modulus of nanocomposite E_{model} versus number of joint elements defined between matrix and zigzag (20,0,20) $(V_n = 2\%)$carbon nanotube in FEA.

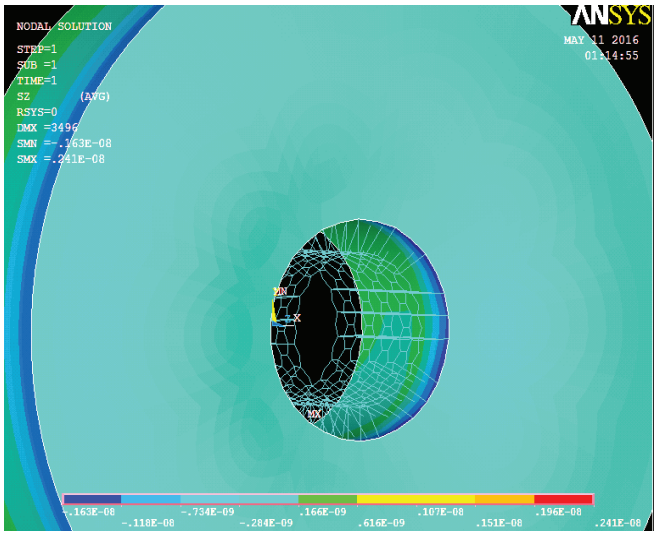

Figure 10. Stress distribution σ_z $\left(N/\overset{\circ}{A}^2\right)$ of composite for $E_m = 3\,GPa$ (zigzag (20,0,20) type nanotube, Young's modulus of the nanotube: $E_n = 1.035 TPa$, radius of the nanotube: $r_n = 9.535\overset{\circ}{A}$, $\left(V_n = 4\%\right)$).

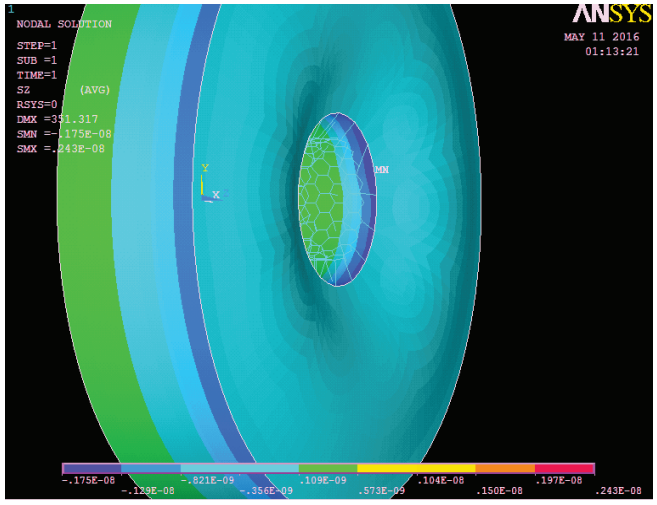

Figure 11. Stress distribution σ_z $\left(N/\overset{\circ}{A}^2\right)$ of composite for , $E_m = 30\,GPa$ (zigzag (20,0,20) type nanotube, Young's modulus of the nanotube $E_n = 1.035 TPa$, radius of the nanotube $r_n = 9.535\overset{\circ}{A}$, $\left(V_n = 4\%\right)$).

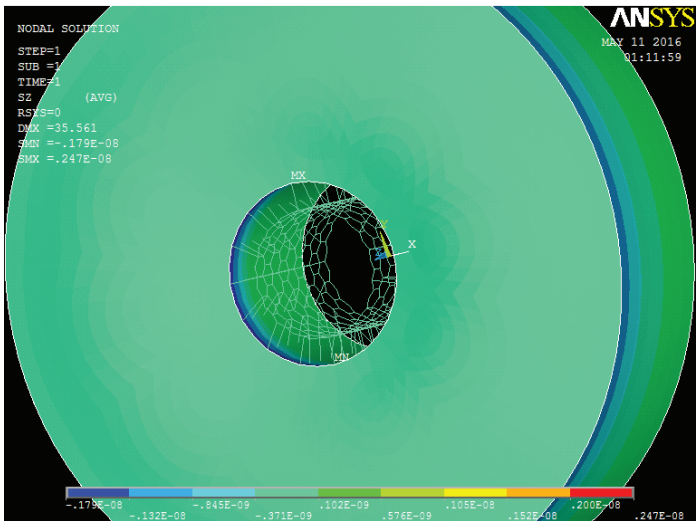

Figure 12. Stress distribution σ_z $\left(N/\mathring{A}^2\right)$ of composite for $E_m = 300\ GPa$ (zigzag (20,0,20) type nanotube, Young's modulus of the nanotube: $E_n = 1.035 TPa$, radius of the nanotube: $r_n = 9.535\mathring{A}$, $\left(V_n = 4\%\right)$).

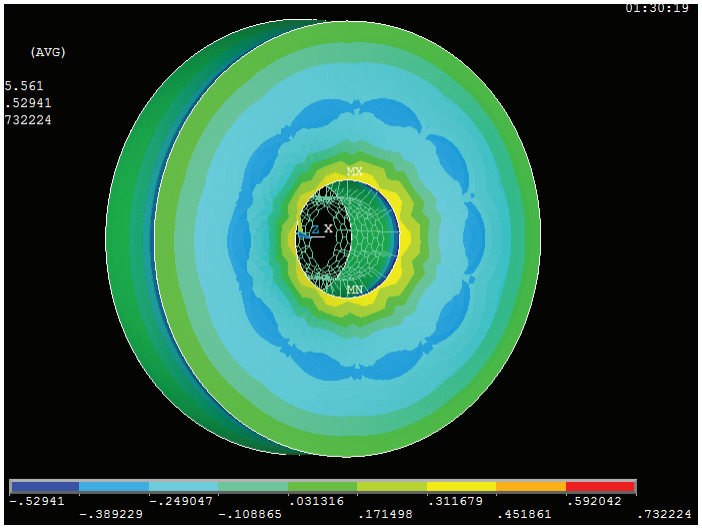

Figure 13. Strain distribution ε_z of composite for $E_m = 300\ GPa$ (zigzag (20,0,20) type nanotube, Young's modulus of the nanotube: $E_n = 1.035 TPa$, radius of the nanotube: $r_n = 9.535\mathring{A}$, $\left(V_n = 4\%\right)$).

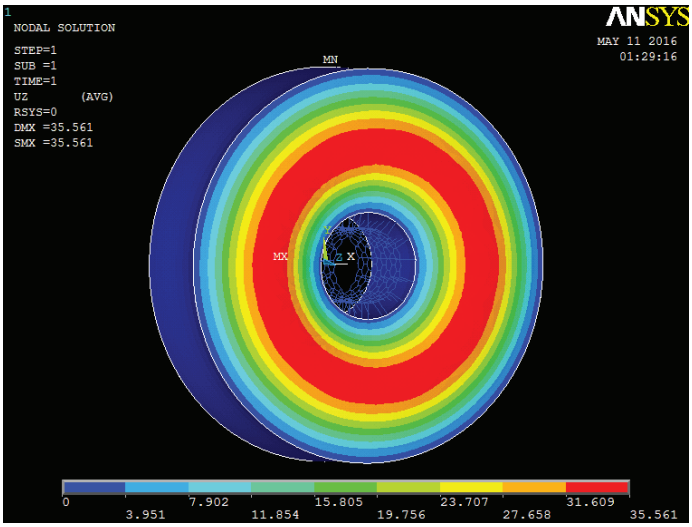

Figure 14. δ_z -displacement distribution of nanocomposite for $E_m = 300GPa$ (zigzag (20,0,20) type nanotube (Young's modulus of the nanotube: $E_n = 1.035TPa$, radius of the nanotube: $r_n = 9.535A^{\circ}$, $(V_n = 4\%)$).

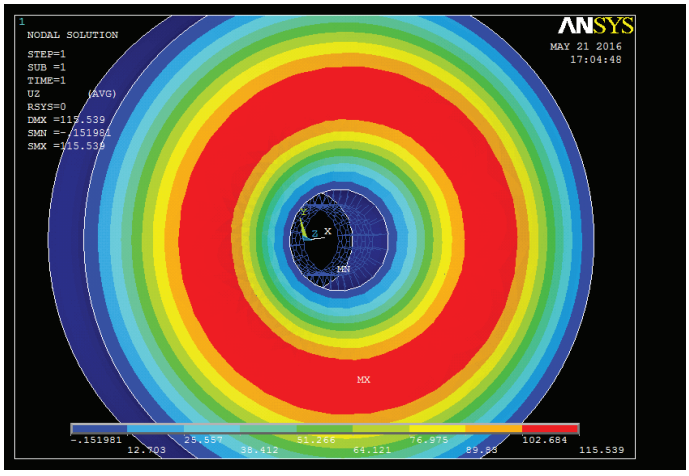

Figure 15. δ_z -displacement distribution of restrained nanocomposite for $E_m = 300GPa$ (zigzag (20,0,20) type nanotube (Young's modulus of the nanotube: $E_n = 1.035TPa$, radius of the nanotube: $r_n = 9.535A^{\circ}$, $(V_n = 2\%)$).

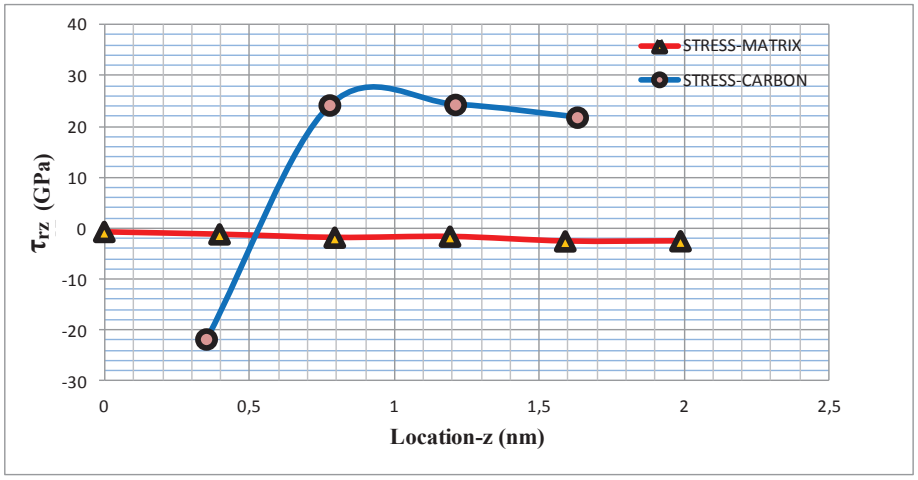

Figure 16. $\tau_{rz}\ \left(N/A^{\circ 2}\right)$ stress distribution within the interface region considering both matrix and carbon nanotube surfaces combined with the joint spring elements of the composite (path-1) ($E_m = 300GPa$ (zigzag (20,0,20) type nanotube $(V_n = 2\%)$).

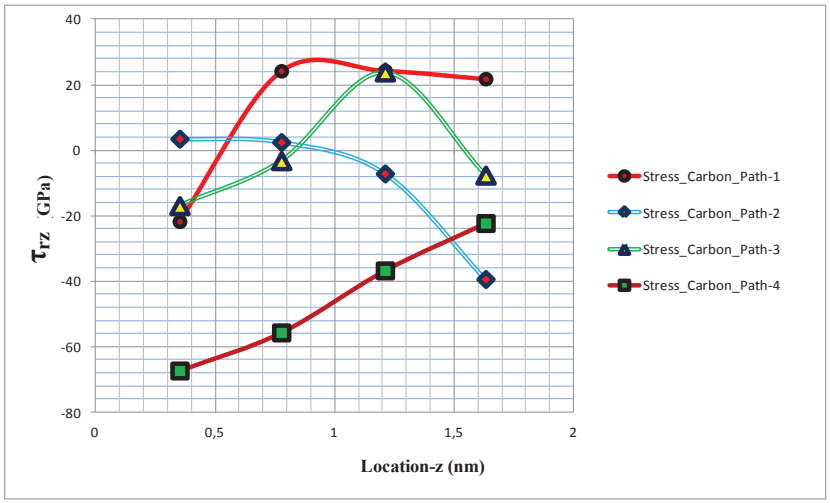

Figure 17. $\tau_{rz}\ \left(N/A^{\circ 2}\right)$ stress distribution within the interface region of the nanocomposite in the consideration of carbon nanotube surfaces (path-1, path-2, path-3, path-4) ($E_m = 300GPa$ (zigzag (20,0,20) type nanotube $(V_n = 2\%)$).

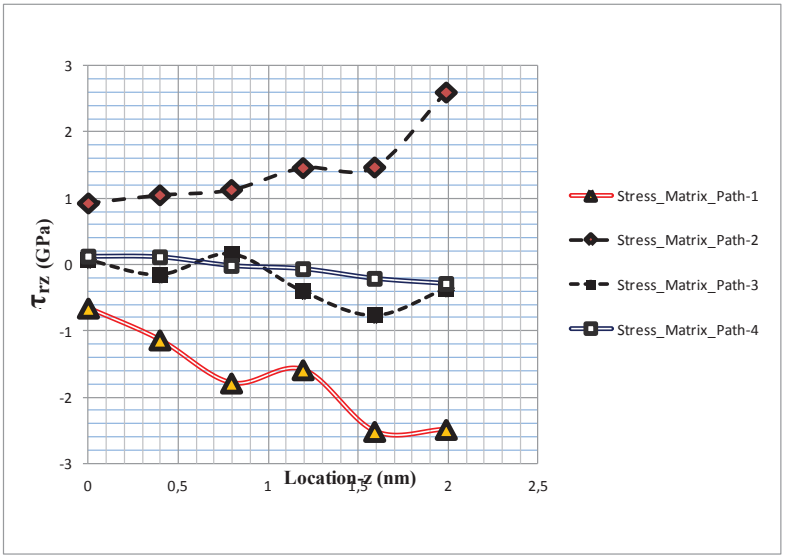

Figure 18. τ_{rz} $\left(N/A^2\right)$ stress distribution within the interface region of the nanocomposite in the consideration of the matrix surfaces (path-1, path-2, path-3, path-4) ($E_m = 300GPa$ (zigzag (20,0,20) type nanotube, $(V_n = 2\%)$).

CONCLUSION

In this study; modeling of the fiber-reinforced composite structure that combines the carbon nanotubes to the matrix with the use of variable number of joint-springs was studied. The solutions obtained from the analysis were summarized in tables and curves. In the FE modeling, carbon nanotubes were selected as zigzag (5,0,20) and zigzag (20,0,20) with the elastic constants of *0.961TPa 1.035TPa* respectively. Matrix material was tested for three different Young's modulus values as; *0.003 TPa, 0.03 TPa, 0.3 TPa* . In the modeling, spring constant was defined as a constant value as *1.13 TPa* . By changing the total number of springs used, different analysis results were obtained and by this way the developed total rigidity of the interface region changed automatically. The research findings have been summarized below;

(1) FE models results were matched with the ROM model values for high elastic constant values of the matrix material [1,4].

(2) The total number of joint-springs used at the interface identification had directly affected the rigidity of the interface region. It may be concluded that the general reaction of the nanocomposite could be changed depending on the applied axial load.

(3) According to the spring element number used in appropriate stiffness values that transmitted the stress values from matrix nodal points to carbon nanotube nodal points were determined by equivalent spring stiffness values.

For example, when two structures combined with 580 joint-springs in parallel connection, the equivalent spring stiffness values were calculated

as $k_{eq} = k_1 + k_2 + .. k_N$ where N represents the number of springs connected the structures. In FE model for $V_n(2\%)$ where each joint-spring has the equal stiffness value $1.33TPa$, generated the equivalent stiffness value of $k_{eq} = 580 \times 1.33TPa = 771\ TPa$ (Table 1-2). In case of parallel connection of springs, obtained total radial stress (force- F_r) and stored potential energy U_r were expressed in terms of radial displacement δ_r as given below respectively.

$$F_r^{eq-spring} = \sum_{i=1}^{N} F_{ri} \tag{4}$$

$$U_r^{eq-spring} = \sum_{i=1}^{N} U_{ri} \tag{5}$$

$$F_r^{eq-sprng} = \sum_{i=1}^{N} k_{ri} \times \delta_{ri} = k_{eq} \times \delta_r \tag{6}$$

Using this modeling procedures, the mechanical behavior of material in nano scale can be predicted by modifying the procedures in FEA as a future work.

ACKNOWLEDGEMENTS

Thanks for the great supports of FIGES and BAP project under grant No. 06/2011-57. This study was performed in Gazi University Ankara, Turkey.

REFERENCES

1. R. S. Ruoff, D. C. Lorents, *Carbon*, **33** (7), 925-930 (1995).

2. G. I. Giannopoulos, S. K. Georgantzinos, N. K. Anifantis, *Composites: Part B*, **41**, 594-601 (2010).

3. A. S. Pour, *Solid State Communications*, **149**, 91-95 (2009).

4. K. N. Spanos, S. K. Georgantzinos, N. K. Anifantis, *Composites: Part B*, **63**, 85-93 (2014).

5. S. K. Georgantzinos, G. J. Giannopoulos, N. K. Anifantis, *Materials and Design*, **31**, 4646-4654 (2010).

6. M. M. Shokrieh, R. Rafiee, *Composite Structures*, **92**, 647-652 (2010).

7. M. M. Shokrieh, R. Rafiee, *Mechanics Research Communications*, **37**, 235-240 (2010).

8. H. Wan, F. Delale, L. Shen, *Mechanics Research Communications*, **32**, 481-489 (2005).

9. L. J. Zhou, Y. L. Kang, J. G. Guo, *Polymer Composites*, 1069-1076 (2011).

10. A. Needleman, T. L. Borders, L. C. Brinson, V. M. F lores, L. S. Schadler, *Composites Science and Technology*, **70**, 2207-2215 (2010).

11. J. L. Tsai, S. H. Tzeng, Y. J. Tzou, *International Journal of Solids and Structures*, **47**, 503-509 (2010).

12. R. S. Ruoff, D. Qian, W. K. Liu, *C. R. Physique*, **4**, 993-1008 (2003).

13. J. P. S. Delmotte, A. Rubio, *Carbon*, **40**, 1729-1734 (2002).

14. A. Pantano, D. M. Parks, M. C. Boyce, *Journal of the Mechanics and Physics of Solids*, **52**, 789-821 (2004).

15. C. Li, T. W. Chou, *Int. J. Solids Struct.*, **40**, 2487-2499 (2003).

16. E. Günay, *AIP Conference Proceedings*, 1727, 020009 (2016).

17. Ç. Akın, M. A. Kışla, E. Günay, Final Project Report, Gazi University Mechanical Eng. Department, Ankara, (2008).

18. E. Günay, Z. Ece, M. A. Esi, *Mechanics of Composite Materials*, **44** (4), 349-360 (2008).

Finite Element Analysis of Stress Transfer Mechanism from Matrix to the Fiber in SWCN Reinforced Nanocomposites

E. Günay

Gazi University, Engineering Faculty, Mechanical Engineering Department, 06570, Maltepe, Ankara, Turkey
Corresponding author: ezgigunay@gazi.edu.tr

Abstract. This study defined as micromechanical finite element (FE) approach examining the stress transfer mechanism in single-walled carbon nanotube (SWCN) reinforced composites. In the modeling, 3D unit-cell method was evaluated. Carbon nanotube reinforced composites were modeled as three layers which comprises CNT, interface and matrix material. Firstly; matrix, fiber and interfacial materials all together considered as three layered cylindrical nanocomposite. Secondly, the cylindrical matrix material was assumed to be isotropic and also considered as a continuous medium. Then, fiber material was represented with zigzag type SWCNs. Finally, SWCN was combined with the elastic medium by using springs with different constants. In the FE modeling of SWCN reinforced composite model springs were modeled by using ANSYS spring damper element COMBIN14. The developed interfacial van der Waals interaction effects between the continuous matrix layer and the carbon nanotube fiber layer were simulated by applying these various spring stiffness values. In this study, the layered composite cylindrical FE model was presented as the equivalent mechanical properties of SWCN structures in terms of Young's modulus. The obtained results and literature values were presented and discussed.

Keywords: Nanotechnology; Carbon nanotube; Fiber-reinforced composites; Interfaces; Finite element analysis.
PACS: 81.07.-b, 61.48.De, 81.05.Ni, 68.35.-p, 02.70.Dh.

INTRODUCTION

Macro and micro studies were evaluated numerically and experimentally, the results were compared as possible. In the literature survey, nano-composites were designed as various forms of multi-layered nano-composites. These multilayered composites were composed of three layers in cylindrical form. These layers were named as follows: matrix material, interface material and fiber material. Each layer consists of a different material type and shows its own physical properties. In the literature, various numerical models were developed appropriate to the structure material in order to find the real structural properties of these layers. Typical bonding methods were used to combine the matrix and fiber in the most suitable form. Considering the researches performed in recent years; single or double-layered carbon nanotubes were seen as a model for fiber reinforcing material. The objective of the

Proceedings of the 6th International Advances in Applied Physics and Materials Science Congress & Exhibition
AIP Conf. Proc. 1809, 020021-1–020021-18; doi: 10.1063/1.4975436
Published by AIP Publishing. 978-0-7354-1477-8/$30.00

most recent studies was to create a new modeling to measure the stress transfer mechanism from fiber to matrix in which the fibers were properly connected.

Basic models were performed using the finite element method. Ruoff et al. [1] investigated the tensile and bending stiffness constants of ideal multi-walled (MWCNT) and single-walled carbon nanotubes (SWCNT) in terms of the known elastic properties of graphite. A semi-continuum finite element approach to evaluate the Young's modulus of single-walled carbon nanotube reinforced composites was investigated by Giannopoulos et al. [2]. In order to accomplish this, a cylindrical representative volume element (RVE) was employed with reinforcement by single walled CNT, the interfacial region represented by spring joint elements and the continuum matrix region by epoxy material. Investigation of stress transfer in carbon nanotube reinforced composites using a multi-scale finite element approach was performed by Spanos et al. [3, 4]. The computation of the elastic mechanical properties of graphene sheets, nanoribbons and graphite flakes using spring based finite element model was performed by Georgantzinos et al. [5]. Shokrieh et al. [6, 7] reported that bonding between carbon nanotube and its surrounding polymer was treated as van der Waals interaction. The results about simulation of carbon nanotube reinforced polymer suggested a non-linear stress-strain behaviour. An equivalent fiber was obtained to calculate the elastic constants of the composite. Wan et al. [8] investigated the effect of CNT length and CNT-matrix interface in single walled carbon nanotube (SWCNT) reinforced composites using continuum model. Zhou et al. [9] reported that the van der Waals pressure between two layers of double walled carbon nanotubes (DWCNT) was introduced in the model, and the Poisson's effects of DWCNT and the matrix were also taken into account by the generalized Hooke's law. Needleman et al. [10] reported that the presence of an interface increased the composite stiffness. However, this interface caused separation and ultimately reduced the stress bearing capacity of the composite. Tsai et al. [11] investigated the characterization of the fracture parameters of a graphene sheet using atomistic simulation and continuum mechanics. Ruoff et al. [12] discussed the mechanical properties of carbon nanotubes by theoretical predictions and experimental measurements. Delmotte et al. [13] reviewed the mechanical properties of carbon nanotubes. Pantano et al. [14] studied on the mechanics of deformation of single and multi-wall carbon nanotubes. Individual tubes were modeled using shell elements, where a specific pairing of elastic properties and mechanical thickness of tube wall were identified to enable successful modeling with shell theory.

The aim of this study was to investigate the effects of spring joint elements as an interface material on the calculation of Young's modulus and the determination of the interface stresses for SWCN reinforced nanotube. The matrix material in tubular form was selected from a homogeneous and continuum medium.The matrix material is being selected from a homogeneous and continuum medium and it has been defined in tubular form. In this research the selected matrix material was epoxy resin. Beside this, fiber material was defined as the discontinuous single walled zigzag type carbon nanotube (SWCN). Two different zigzag type nanotubes (5,0,20) and (20,0,20) were introduced as a fiber geometry and material. Matrix and fiber geometries were connected to each other with the help of springs in place of van der Waals bonds. The

developed interfacial van der Waals interaction effects between the matrix layer and the carbon nanotube fiber layer were simulated by finite element method.

MICROMECHANICAL MODELLING

All of the computations were performed in a representative volume element (RVE) which consists of matrix, interface joint spring elements and single wall carbon nanotube (Fig. 1). The geometric parameters of the RVE were determined from the Eqn. 1 and Eqn. **2** given as below. In these equations V_n, V_{CNT}, V_m were the volume fractions of the CNT in the composite with respect to the proposed RVE, volume fraction of the nanotube and volume fraction of matrix material respectively. The parameters r_n, r_m presented the radius of the nanotube and matrix, t_n the nanotube with 0.34 nm wall thickness [2, 15] ; l_n represented the nanotube length. $E_c\left(\vdots E_c^*\right)$ showed the Young's modulus of the nanocomposite which was approximately predicted by Eqn. 2. In this study, construction of the fiber-reinforced composite structure was formed with the combination of the carbon nanotube and joint-springs in order to represent the fiber structure. The interface between matrix and carbon nanotubes was represented with the help of different number of springs with high stiffness properties. By applying this equation (**R**ule of **M**ixtures: ROM) effective Young's modulus of the fiber-reinforced composite was estimated in the fiber direction.

$$V_n = \frac{V_{CNT}}{V_{matrix}+V_{CNT}} = \frac{2\pi r_n t_n l_n}{\left\{\pi\left[r_m^2-(r_n+t_n/2)^2\right]l_n+2\pi r_n t_n l_n\right\}} = \frac{8 r_n t_n}{4r_m^2-(t_n-2r_n)^2} \tag{1}$$

$$E_c = E_n V_n + (1-V_n)E_m \tag{2}$$

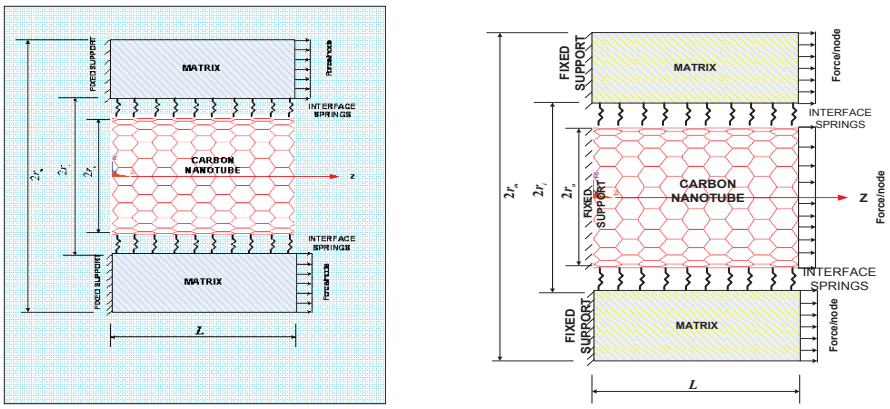

a) b)

Figure 1. Representative volume element (RVE) of zigzag type carbon nanotube with joint-springs reinforced composite: a) BC_1: loading applied from matrix; b) BC_2: loading applied from both matrix and carbon nanotube.

The radius of matrix r_m was solved using the Eqn. 1 with corresponding volume fractions of 1%-4%. The calculated Young's modulus and radii values of the zigzag nanotubes (5,0,20) (Fig. 2), (20,0,20) (Fig. 3) were $E_n = 0.961 TPa$, $r_n = 1.9586 A^{\circ}$ and $E_n = 1.035 TPa$, $r_n = 9.535 A^{\circ}$ respectively (Table 1, Table 2).

Table 1. FE models with zigzag (5,0,20) type carbon nanotube and number of elements with their types.

Volume Fraction $(V_n)\%$	Radius of the matrix $(r_m)\ A^{\circ}$	Mesh elements (Matrix) SHELL181	Mesh elements (Reinforcing Springs) COMBIN14	Mesh elements (Carbon nanotube) BEAM4
1	11.543	1105	103	145
2	8.165	639, 3159	120, 580	145, 121
3	6.668	599	99	145
4	5.780	479	99	145

Table 2. FE models with zigzag (20,0,20) type carbon nanotube and number of elements with their types.

Volume Fraction $(V_n)\%$	Radius of the matrix $(r_m)\ A^{\circ}$	Mesh elements (Matrix) SHELL181	Mesh elements (Reinforcing Springs) COMBIN14	Mesh elements (Carbon nanotube) BEAM4
1	80.755	3626	138	580
2	57.474	7902	447	580
3	47.145	2059	166	580
4	41.016	2819	221	580

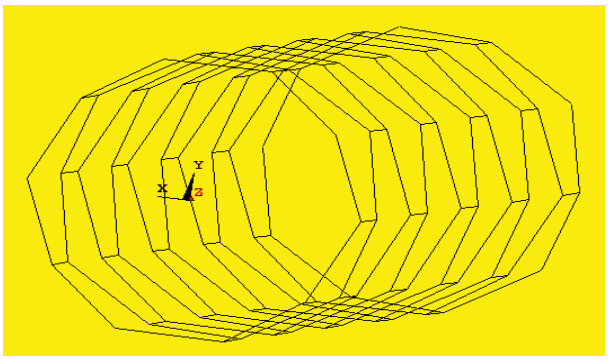

Figure 2. Meshing of zigzag (5,0,20) type carbon nanotube.

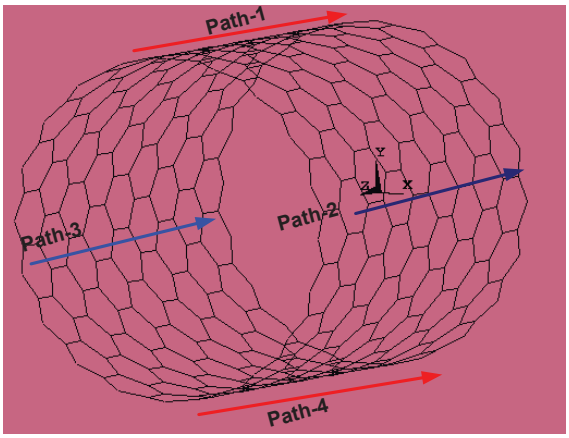

Figure 3. Meshing of zigzag (20,0,20) type carbon nanotube.

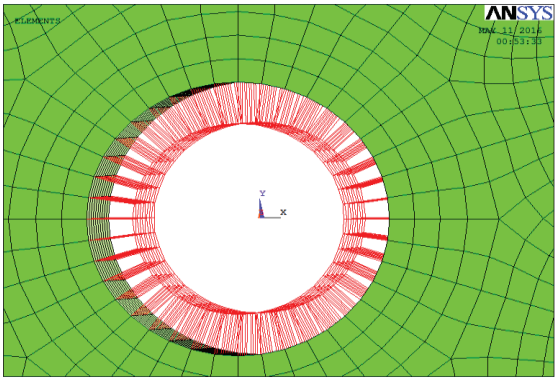

Figure 4. Zigzag (20,0,20) type nanotube-Combin14 spring elements -Shell181 mesh elements combination (Young's modulus of the nanotube $E_n = 1.035TPa$, radius of the nanotube $r_n = 9.535A^{\circ}$, $(V_n)\% = 2$).

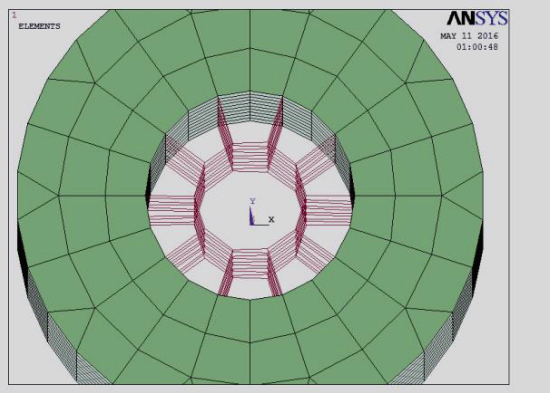

Figure 5. Zigzag (5,0,20) type nanotube-Combin14 spring elements -Shell181 mesh elements combination (Young's modulus of the nanotube $E_n = 0.961 TPa$, radius of the nanotube $r_n = 1.9586 A^{\circ}$, $(V_n)\% = 2$).

Carbon nanotubes were generated from two-nodes **BEAM 3-D elastic 4** element with the properties given in detail in Table 3 [16, 17] (Fig. 2, Fig. 3). Element has six degrees of freedom per node (UX, UY, UZ, ROTX, ROTY, ROTZ). Carbon nanotube elastic constants were calculated as $k_{carbon} = 0.961\, TPa$ and $k_{carbon} = 1.035 TPa$. The thickness of the interface section was equal to one half of the wall thickness of the nanotube $(t_n/2)$[2, 15], and usually taken as equal to 3.4 Å. The matrix section of the composite was considered to be a continuous structure such as epoxy material, and comparison of the results were done for three different values of elstic constants of matrix material (Table 4). $E_{matrix} = k_{matrix} = 3GPa,\ E_{matrix} = k_{matrix} = 30\, GPa$ and $E_{matrix} = k_{matrix} = 300\, GPa$ (Table 4). The matrix was modelled by using four-node linear mesh element **SHELL181** with six degrees of freedom per node (UX, UY, UZ, ROTX, ROTY, ROTZ) (Fig. 4). **COMBIN14** mesh element has three degrees of freedom per node (UX, UY, UZ) (Fig. 5). Stiffness value of the springs was chosen as $k_{spring} = k_s = 1.33\, TPa$ and this value was defined for **COMBIN14** mesh element. Finite element analyses were performed for five different stiffness ratios as,

$$k_i / k_s = 2.255 \times 10^{-3},\ 2.255 \times 10^{-2},\ 2.255 \times 10^{-1},\ 3.1217 \times 10^{-3},\ 2.8985 \times 10^{-3}$$

(Table 5, Table 6).

Table 3. Carbon nanotube BEAM 3-D Elastic-4 beam section properties.

A	1.697e-8 A° ^{2}
I_{zz}	0.227 A° ^{4}
I_{yy}	0.227 A° ^{4}
t_z	0.147 A° ^{4}
t_y	0.147 A° ^{4}
I_{xx}	0.453 A° ^{4}
E_x	5.49e-8 N/A°^{2}
E_y	5.49e-8 N/A°^{2}
E_z	5.49e-8 N/A°^{2}
G_{xy}	8.71 e-9 N/A°^{2}
G_{yx}	8.71 e-9 N/A°^{2}
G_{xz}	8.71 e-9 N/A°^{2}

COMPUTATIONAL PROCEDURES

This study was performed mainly in two steps. In the first step, the Young's modulus of the nanocomposite structure was calculated in which the composite structure was loaded axially. At one end of the cylinder (RVE) only the nodes of the matrix profile were fully restrained, i.e., the degrees of freedom of all nodes of this surface were restricted. At the other end of the cylinder (RVE), a constant force per node was applied at the nodes of the circular cross sectional face of the matrix (Fig. 1(a)). The back and front faces of the carbon nanotube were neither supported nor loaded, they were released free of loading (Boundary Condition type 1: BC_1). By this way it was allowed the stiffness effect of the carbon nanotube to be transferred to the matrix through the interconnection springs. The Young's modulus value of the nanocomposite was calculated from the ANSYS code nodal solution with the replacement of the values in the following Hooke's formula:

$$E_c = \left[\frac{\left(\sigma_z^{node}\right)_{max}}{\left(\varepsilon_z^{node}\right)_{max}} \right]_{Loaded\ face} \tag{3}$$

In the second stage of this study, stress distribution formed between the matrix and carbon nanotube was calculated under the similar axial loading applications. At one end of the cylinder (RVE) both the nodes of the matrix profile and carbon nanotube were fully restrained, i.e. the degrees of freedom of all nodes of this surface were restricted (Boundary Condition type 2: BC_2). At the other end of the RVE, nanocomposite was loaded with a constant force per node (Fig. 1(b)).

FE ANALYSIS RESULTS

The first step in application was performed with the boundary condition BC_1 and $V_n(1\%-4\%)$ type nanocomposite cylinders. The results obtained from the modeling and analysis can be viewed from in the Table 4 and Table 5. The curves of these data have shown in the Figure 6 and Figure 7. The elastic constant of the matrix material was considered as $E_{matrix}=3GPa$ then, the values obtained from FEM model and the ROM model (E_{ROM}/E_m) were compared with each other. According to this comparison $4.5-18.5$ relative difference was found between them. . By proceeding ROM model and the matrix material with Young's modulus on the same curve, the proportion of these two values was found and the curve was plotted. Approximate difference between the ROM model and the matrix material was $0.98-1.2$ .The increasing difference between the FEM model and ROM model was found to be proportional to the increase in the volume fraction of fiber in matrix. The increasing difference between the FEM model and ROM model was found to be proportional to the increase in the value of the volume fraction of fiber in matrix. These results were found to be consistent with the literature [2]. Zigzag (5,0,20) and zigzag (20,0,20) carbon nanotubes gave similar results in terms of the equivalent elastic constants of nanocomposite structures. The differences obtained by studying the two reinforcing structures that affected the general structure of the composite was shown in Fig. 7. The equivalent composite elastic constants obtained from FE analysis by inserting the matrix material elastic constants $3GPa$, $30GPa$ and $300GPa$ were shown in Fig. 8 respectively. According to these results it was found that, when the matrix material has the largest elastic constant ($300GPa$) both the carbon nanotube model and the ROM model have shown aproximately same values. The differences caused by the selected carbon nanotube reinforced composite structure have been observed between $1-1.2$ factors $(E_{matrix}=3GPa)$ (Fig.9).

According to our results, the biggest effects developed on the equivalent elastic constant of the reinforced nanocomposite have obtained from the following parameters; (i) the equivalent elastic constant value of carbon nanotube, (ii) the number of series of joint spring elements and their corresponding stiffness values, (ii) the defined matrix material with its geometrical and material properties (Figs. 6-9).

The stress (σ_z), strain (ε_z), and displacement (δ_z) based curves obtained from Ansys code for zigzag (20,0,20) type nanotube (Young's modulus of the nanotube: $E_n=1.035TPa$, radius of the nanotube: $r_n=9.535A^\circ$, $\left(r_m=5.780A^\circ\right),(V_n=4\%)$) have been shown in Figures 10-14. The developing z directional stress distribution plots (σ_z) on the unrestricted (BC_1,Fig.1(a)) reinforced nanocomposite as; $3GPa$, $30GPa$ and $300GPa$ matrix models have been shown in Figures 10, 11 and 12 respectively. The strain distribution (ε_z) for $300GPa$ has been shown in Figure 13, the z directional displacement distribution for $300GPa,(\delta_z)$ has been shown in Fig. 14 and the δ_z - displacement distribution of restrained (BC_2, Fig. 1(b)) nanocomposite for $E_m=300GPa$ (zigzag (20,0,20) type nanotube (Young's modulus of the nanotube: $E_n=1.035TPa$, radius of the nanotube: $r_n=9.535A^\circ$, $\left(r_m=8.165A^\circ\right),(V_n=2\%)$) has been

shown in Fig. 15. As seen in Figure 14 and Figure 15, the relative minimum value of the z-displacement (δ_z) occured in the interface region where the joint-springs were aligned there. The other results obtained from the examination of interface shear stress distribution (τ_{rz}) by applying the second type of boundary condition (BC_2) on the FE model by have been shown in Figs. 16, 17 and 18. Figure 16 has shown clearly the interfacial shear stress distribution formed between the matrix and carbon nanotube [18]. The plotted nodal shear stress values were obtained from nodal solution of matrix section (Shell181 elements) while the corresponding axial stresses obtained from the carbon nanotube by ANSYS Beam-4 elements at same locations of the meshing system. As it is shown in the Figs. 16, 17 and 18, the carrying capacity of the matrix was found to be 33.3% of the total load carrying capacity of the modelled composite structure. The load carrying capacity of the springs and carbon nanotube together was 66.7% of the overall load carrying capacity of the modeled composite structure.

Table 4. FEA results for zigzag (5,0,20) type nanotube (Young's modulus of the nanotube $E_n = 0.96 ITPa$, radius of the nanotube $r_n = 1.9586 A^{\circ}$).

Volume Fraction $(V_n)\%$	**Present model** $E_c(GPa)$	**Rule of mixtures** $E_c^*(GPa)$	**Matrix material** $E_m(GPa)$	**Elastic constants ratio** E_c^*/E_c
1	3.205	12.58	3.0	3.925
2	3.1013	22.16	3.0	7.145
3	3.569	31.74	3.0	8.893
4	2.946	41.32	3.0	14.026

Table 5. FEA results for zigzag (20,0,20) type nanotube (Young's modulus of the nanotube $E_n = 1.035 TPa$, radius of the nanotube $r_n = 9.535 A^{\circ}$).

Volume Fraction $(V_n)\%$	**Present model** $E_c(GPa)$	**Rule of mixtures** $E_c^*(GPa)$	**Matrix material** $E_m(GPa)$	**Elastic constants ratio** E_c^*/E_c
1	2.398	13.32	3.0	5.555
2	3.409	23.64	3.0	6.935
3	3.379	33.96	3.0	10.050
4	3.324	44.28	3.0	13.321

Table 6. FEA results for zigzag (20,0,20) type nanotube (Young's modulus of the nanotube $E_n = 1.035 TPa$, radius of the nanotube $r_n = 9.535 A^{\circ}$ and volume fractions; $V_n = 4\%$, $V_n = 2\%$).

Matrix material $E_m(GPa)$	**Present model** $V_n = 2\%$ $E_c(GPa)$	**Present model** $V_n = 4\%$ $E_c(GPa)$	**Rule of mixtures** $E_c^*(GPa)$	**Elastic constants ratio** $V_n = 2\%$ E_c^*/E_c	**Elastic constants ratio** $V_n = 4\%$ E_c^*/E_c
3	3.48	3.19	44.28	6.79	13.88
30	34.69	34.22	70.20	1.16	2.05
300	345.54	345.0	329.4	0.91	0.96

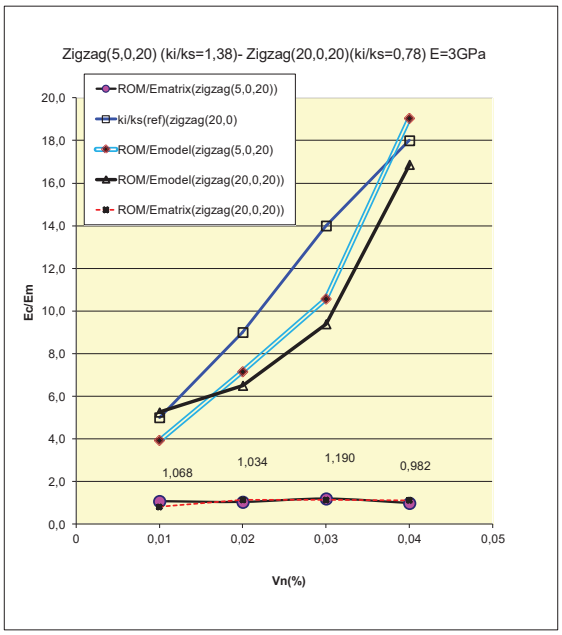

Figure 6. Comparison of **FEA** results ROM/E_{matrix} and $ROM/E_{mod\,el}$ versus volume fraction $(V_n\%)$ for zigzag (5,0,20) and (20,0,20) type reinforced nanocomposites.

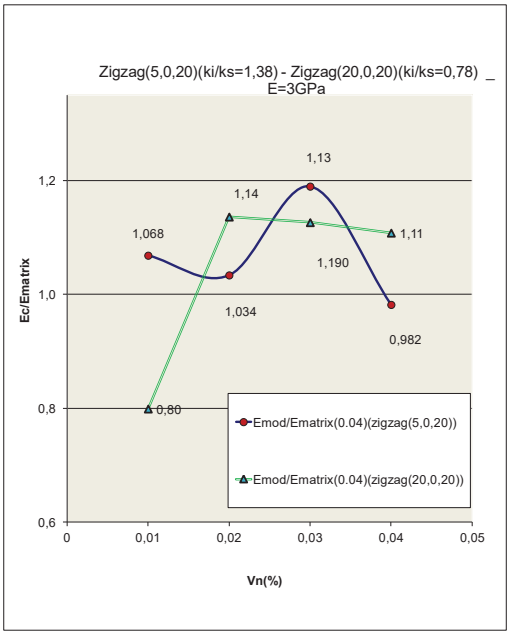

Figure 7. Comparison of the FEA results for $E_{mod\,el}/E_{matrix}$ versus volume fraction $(V_n\%)$ for zigzag (5,0,20) and (20,0,20) type reinforced nanocomposites.

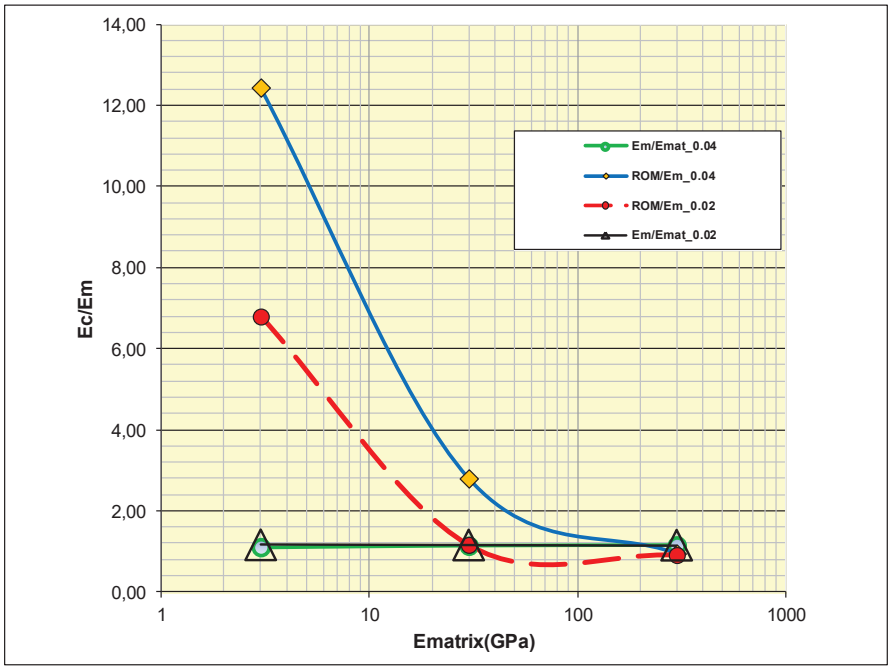

Figure 8. Comparison of FEA results ROM/E_{matrix} and $ROM/E_{mod\,el}$ versus E_{matrix} for zigzag (5,0,20) and zigzag(20,0,20) type reinforced nanocomposites.

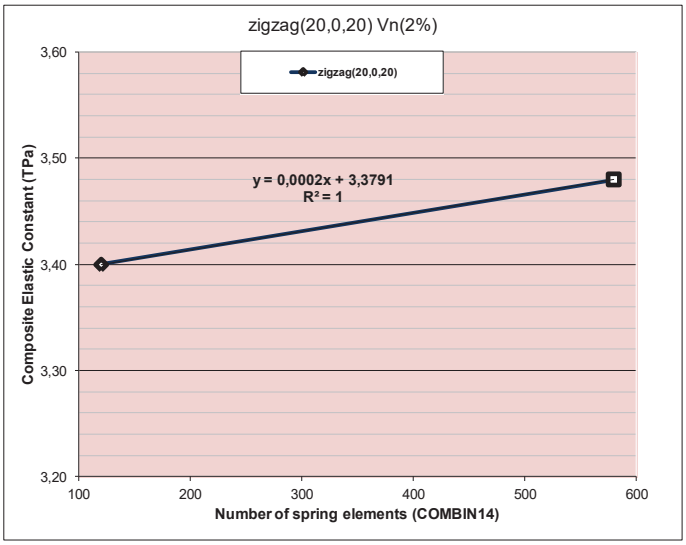

Figure 9. Variation of Young's modulus of nanocomposite $E_{mod\,el}$ versus number of joint elements defined between matrix and zigzag (20,0,20) $(V_n = 2\%)$carbon nanotube in FEA.

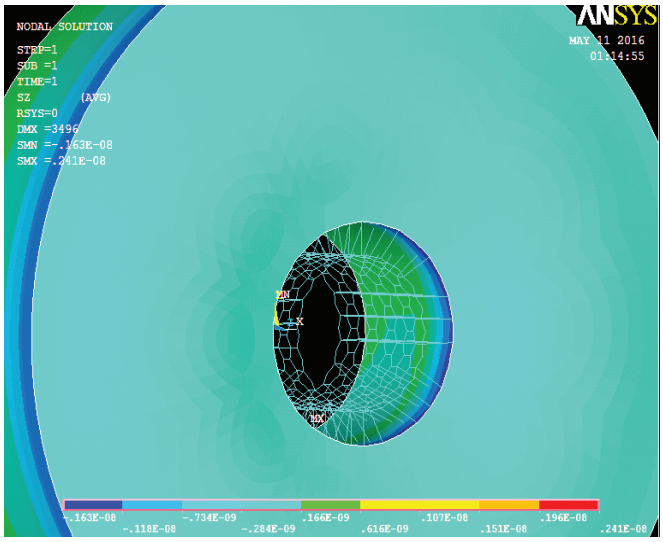

Figure 10. Stress distribution $\sigma_z \left(N/\overset{\circ}{A}^2 \right)$ of composite for $E_m = 3\,GPa$ (zigzag (20,0,20) type nanotube, Young's modulus of the nanotube: $E_n = 1.035\,TPa$, radius of the nanotube: $r_n = 9.535\overset{\circ}{A}$, $(V_n = 4\%)$).

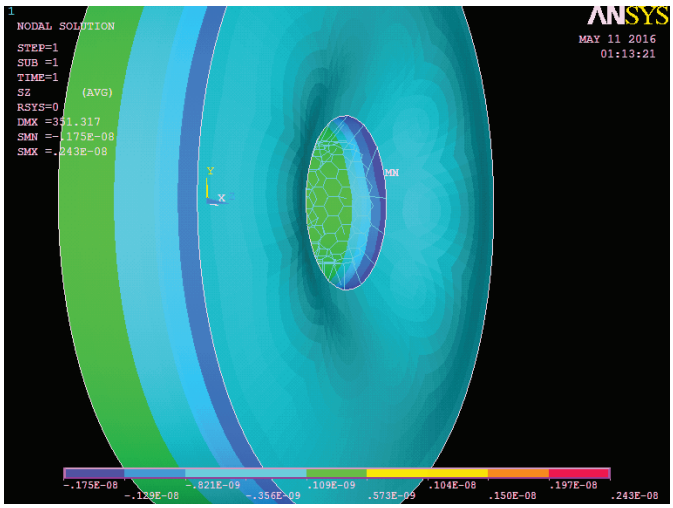

Figure 11. Stress distribution $\sigma_z \left(N/\overset{\circ}{A}^2 \right)$ of composite for , $E_m = 30\,GPa$ (zigzag (20,0,20) type nanotube, Young's modulus of the nanotube $E_n = 1.035\,TPa$, radius of the nanotube $r_n = 9.535\overset{\circ}{A}$, $(V_n = 4\%)$).

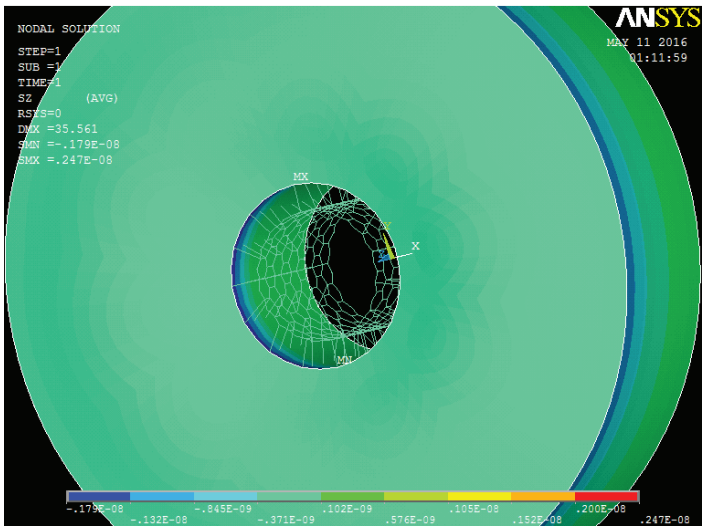

Figure 12. Stress distribution σ_z $\left(N/\mathring{A}^2\right)$ of composite for $E_m = 300\,GPa$ (zigzag (20,0,20) type nanotube, Young's modulus of the nanotube: $E_n = 1.035\,TPa$, radius of the nanotube: $r_n = 9.535\,\mathring{A}$, $\left(V_n = 4\%\right)$).

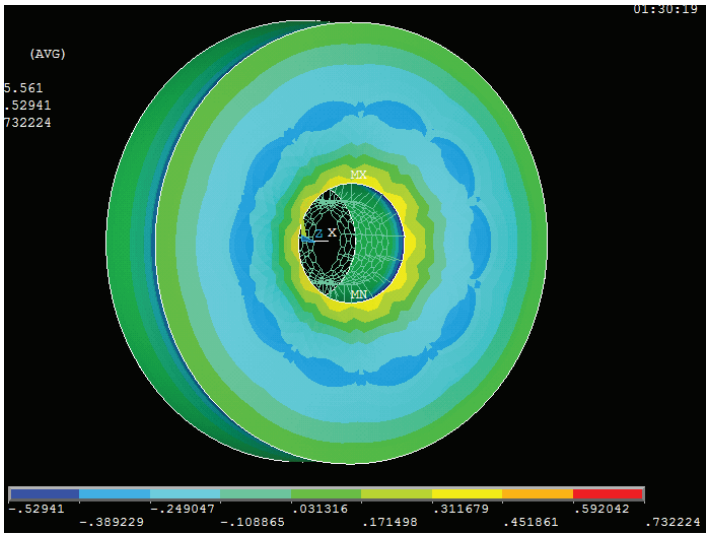

Figure 13. Strain distribution ε_z of composite for $E_m = 300\,GPa$ (zigzag (20,0,20) type nanotube, Young's modulus of the nanotube: $E_n = 1.035\,TPa$, radius of the nanotube: $r_n = 9.535\,\mathring{A}$, $\left(V_n = 4\%\right)$).

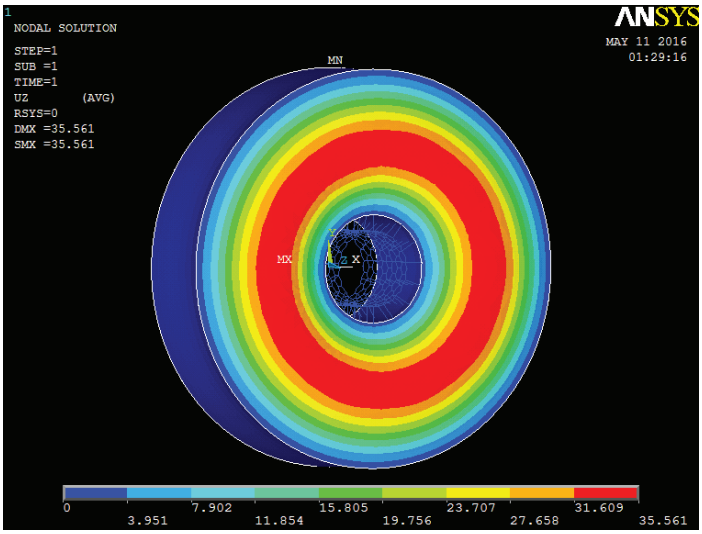

Figure 14. δ_z -displacement distribution of nanocomposite for $E_m = 300GPa$ (zigzag (20,0,20) type nanotube (Young's modulus of the nanotube: $E_n = 1.035\,TPa$, radius of the nanotube: $r_n = 9.535\,A^{\circ}$, $(V_n = 4\%)$).

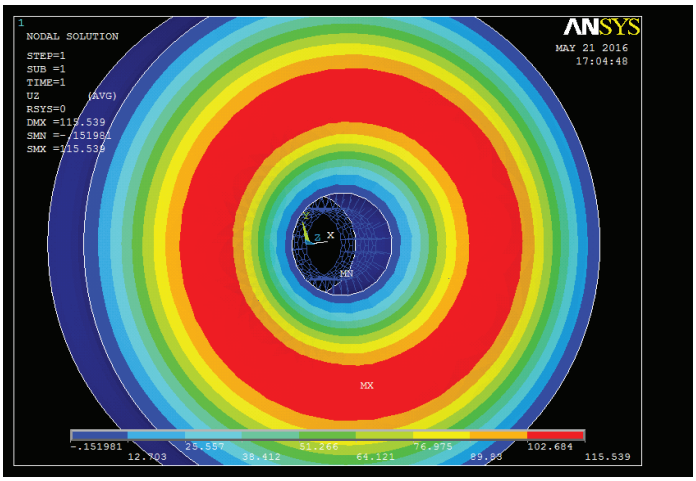

Figure 15. δ_z -displacement distribution of restrained nanocomposite for $E_m = 300GPa$ (zigzag (20,0,20) type nanotube (Young's modulus of the nanotube: $E_n = 1.035\,TPa$, radius of the nanotube: $r_n = 9.535\,A^{\circ}$, $(V_n = 2\%)$).

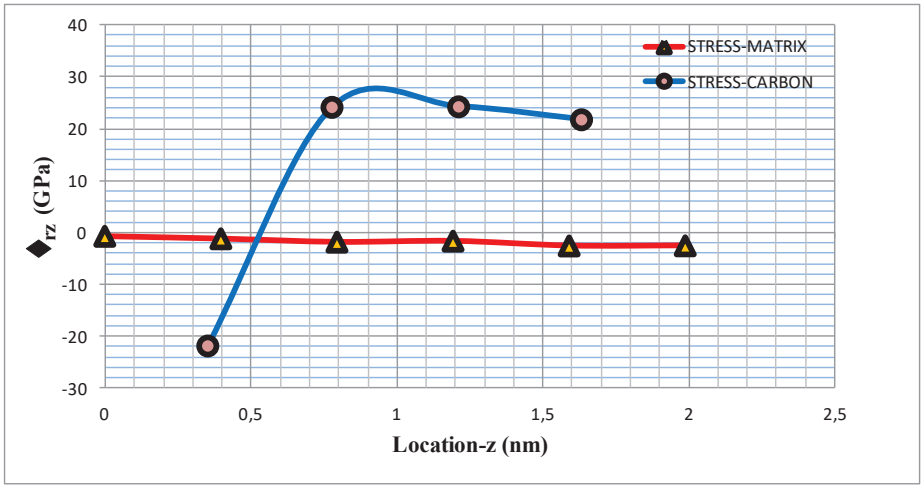

Figure 16. τ_{rz} $\left(N/A^{\circ 2}\right)$ stress distribution within the interface region considering both matrix and carbon nanotube surfaces combined with the joint spring elements of the composite (path-1) ($E_m = 300GPa$ (zigzag (20,0,20) type nanotube $(V_n = 2\%)$).

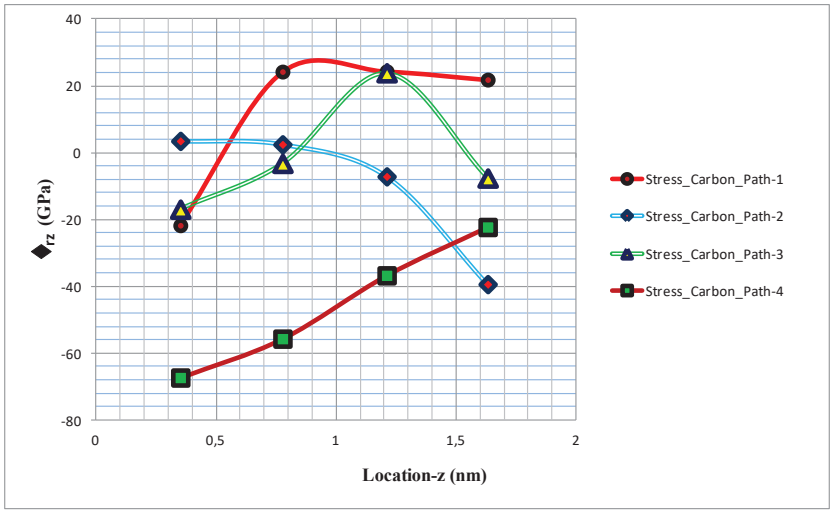

Figure 17. τ_{rz} $\left(N/A^{\circ 2}\right)$ stress distribution within the interface region of the nanocomposite in the consideration of carbon nanotube surfaces (path-1, path-2, path-3, path-4) ($E_m = 300GPa$ (zigzag (20,0,20) type nanotube $(V_n = 2\%)$).

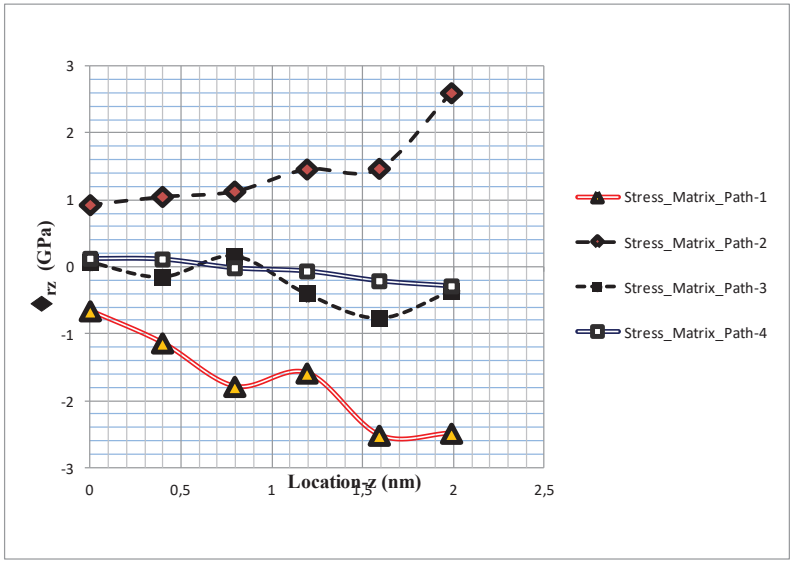

Figure 18. τ_{rz} $\left(N/A^2\right)$ stress distribution within the interface region of the nanocomposite in the consideration of the matrix surfaces (path-1, path-2, path-3, path-4) ($E_m = 300GPa$ (zigzag (20,0,20) type nanotube, $(V_n = 2\%)$).

CONCLUSION

In this study; modeling of the fiber-reinforced composite structure that combines the carbon nanotubes to the matrix with the use of variable number of joint-springs was studied. The solutions obtained from the analysis were summarized in tables and curves. In the FE modeling, carbon nanotubes were selected as zigzag (5,0,20) and zigzag (20,0,20) with the elastic constants of $0.96ITPa$ $1.035TPa$ respectively. Matrix material was tested for three different Young's modulus values as; $0.003TPa, 0.03TPa, 0.3TPa$. In the modeling, spring constant was defined as a constant value as $1.13TPa$. By changing the total number of springs used, different analysis results were obtained and by this way the developed total rigidity of the interface region changed automatically. The research findings have been summarized below;

(1) FE models results were matched with the ROM model values for high elastic constant values of the matrix material [1,4].

(2) The total number of joint-springs used at the interface identification had directly affected the rigidity of the interface region. It may be concluded that the general reaction of the nanocomposite could be changed depending on the applied axial load.

(3) According to the spring element number used in appropriate stiffness values that transmitted the stress values from matrix nodal points to carbon nanotube nodal points were determined by equivalent spring stiffness values.

For example, when two structures combined with 580 joint-springs in parallel connection, the equivalent spring stiffness values were calculated as

$k_{eq} = k_1 + k_2 + ...k_N$ where N represents the number of springs connected the structures. In FE model for $V_n(2\%)$ where each joint-spring has the equal stiffness value $1.33TPa$, generated the equivalent stiffness value of $k_{eq} = 580 \times 1.33TPa = 771TPa$ (Table 1-2). In case of parallel connection of springs, obtained total radial stress (force-F_r) and stored potential energy U_r were expressed in terms of radial displacement δ_r as given below respectively.

$$F_r^{eq-spring} = \sum_{i=1}^{N} F_{ri} \tag{4}$$

$$U_r^{eq-spring} = \sum_{i=1}^{N} U_{ri} \tag{5}$$

$$F_r^{eq-sprng} = \sum_{i=1}^{N} k_{ri} \times \delta_{ri} = k_{eq} \times \delta_r \tag{6}$$

Using this modeling procedures, the mechanical behavior of material in nano scale can be predicted by modifying the procedures in FEA as a future work.

ACKNOWLEDGEMENTS

Thanks for the great supports of FIGES and BAP project under grant No. 06/2011-57. This study was performed in Gazi University Ankara, Turkey.

REFERENCES

1. R. S. Ruoff, D. C. Lorents, *Carbon*, **33** (7), 925-930 (1995).

2. G. I. Giannopoulos, S. K. Georgantzinos, N. K. Anifantis, *Composites: Part B*, **41**, 594-601 (2010).

3. A. S. Pour, *Solid State Communications*, **149**, 91-95 (2009).

4. K. N. Spanos, S. K. Georgantzinos, N. K. Anifantis, *Composites: Part B*, **63**, 85-93 (2014).

5. S. K. Georgantzinos, G. J. Giannopoulos, N. K. Anifantis, *Materials and Design*, **31**, 4646-4654 (2010).

6. M. M. Shokrieh, R. Rafiee, *Composite Structures*, **92**, 647-652 (2010).

7. M. M. Shokrieh, R. Rafiee, *Mechanics Research Communications*, **37**, 235-240 (2010).

8. H. Wan, F. Delale, L. Shen, *Mechanics Research Communications*, **32**, 481-489 (2005).

9. L. J. Zhou, Y. L. Kang, J. G. Guo, *Polymer Composites*, 1069-1076 (2011).

10. A. Needleman, T. L. Borders, L. C. Brinson, V. M. F lores, L. S. Schadler, *Composites Science and Technology*, **70**, 2207-2215 (2010).

11. J. L. Tsai, S. H. Tzeng, Y. J. Tzou, *International Journal of Solids and Structures*, **47**, 503-509 (2010).

12. R. S. Ruoff, D. Qian, W. K. Liu, *C. R. Physique*, **4**, 993-1008 (2003).

13. J. P. S. Delmotte, A. Rubio, *Carbon*, **40**, 1729-1734 (2002).

14. A. Pantano, D. M. Parks, M. C. Boyce, *Journal of the Mechanics and Physics of Solids*, **52**, 789-821 (2004).

15. C. Li, T. W. Chou, *Int. J. Solids Struct.*, **40**, 2487-2499 (2003).

16. E. Günay, *AIP Conference Proceedings*, 1727, 020009 (2016).

17. Ç. Akın, M. A. Kışla, E. Günay, Final Project Report, Gazi University Mechanical Eng. Department, Ankara, (2008).

18. E. Günay, Z. Ece, M. A. Esi, *Mechanics of Composite Materials*, **44** (4), 349-360 (2008).